Clim Dyn
DOI 10.1007/s00382-009-0695-4

Scale-decomposed atmospheric water budget over North America as simulated by the Canadian Regional Climate Model for current and future climates

Raphaël Bresson · René Laprise

Received: 22 May 2009 / Accepted: 21 October 2009

Abstract Through its various radiative effects and latent heat release, water plays a major role in the maintenance of climate. Therefore a better understanding of climate and climate changes requires a better understanding of the hydrological cycle. In this study we investigate the scale-decomposed atmospheric water budget over North America as simulated by the Canadian Regional Climate Model (CRCM) driven by the Canadian Coupled Global Climate Model (CGCM) under current conditions for 1961–1990 and the SRES A2 scenario for 2041–2070. A discrete cosine transform is applied to the atmospheric water budget variables in order to separate small scales that are resolved exclusively by the high-resolution CRCM, from larger scales resolved by both the CRCM and low-resolution driving CGCM. The moisture flux divergence is alternatively decomposed in terms of three scales of wind and humidity to provide nine interaction terms. Statistics of these fields are calculated for winter and summer seasons, and the local statistical significance of climate-change projections is tested. The contributions of each scale band to the water budget current climatology and to its evolution in a warmer climate are investigated, addressing the issue of the potential added value of smaller scales. Results show a time variability larger than the time mean for all variables, and a significant small-scale contribution to time variability, which is even dominant in summer, both in the current and future climates. Future climate exhibits an overall intensification of the hydrological cycle in winter, and more mixed changes in summer. Relative changes in the time mean and time variability appear comparable, and the contribution of each scale band to variability changes remains overall very consistent with their contribution to current climate variability.

Keywords Regional climate model · Scale decomposition · Atmospheric water budget · Climate change · Added value

1 Introduction

Water plays a major role in the climate system. It contributes to heat transport from warm regions with excess evapotranspiration over precipitation, to cold regions with excess precipitation over evapotranspiration, through evaporative cooling at the surface and latent heat release heating the atmosphere. Water also strongly affects solar and terrestrial radiation transfers with its radiative properties that change widely with its phases (in the atmosphere as water vapour, cloud water droplets and ice crystals of various sizes, and at the surface with liquid water, ice and snow). River runoff influences the salinity of coastal water and constitutes a fresh-water forcing that affects ocean currents. Several water-related feedbacks appear to be of primary importance in the maintenance of climate. Therefore a good understanding of the hydrological cycle is essential for a proper representation of the current climate and its future evolution (e.g., GEWEX, Lawford et al. 2004, 2007).

The atmospheric and terrestrial branches of the hydrological cycle are linked through precipitation and evapotranspiration (Peixoto and Oort 1992). The closure of the

R. Bresson · R. Laprise (✉)
Canadian Regional Climate Modelling and Diagnostics (CRCMD) Network, Centre ESCER (Étude et Simulation du Climat à l'Échelle Régionale), University of Quebec at Montreal, PO Box 8888, Stn. Centre-Ville, Montreal, QC H3C 3P8, Canada
e-mail: laprise.rene@uqam.ca

Published online: 02 December 2009

surface hydrological budget with atmospheric variables can thus be useful to estimate surface variables that are poorly known because they are difficult, sometimes nearly impossible, to measure with sufficient resolution and accuracy (Music and Caya 2007, 2009).

In spite of their importance, several basic atmospheric hydrological variables are still poorly observed. In situ precipitation measurements are taken at irregular and sometimes widely spaced locations and they suffer from several errors (windy weather, snow precipitation). Before satellites, atmospheric moisture storage and transport were calculated from widely spaced radiosonde measurements. Evapotranspiration is not routinely measured but it is deduced from other variables. Thus observations can fail at providing the relevant information required with sufficient space and time resolution. High-resolution climate models can possibly constitute a tool to generate information about hydrological cycle components that are difficult to measure (e.g., Laprise 2008).

Under scenarios of increased greenhouse gases, climate models project an overall intensification of the hydrological cycle (Trenberth 1999a; Trenberth et al. 2003; Allen and Ingram 2002; Christensen et al. 2007). This in part results from the increased water-holding capacity with temperature following the Clausius–Clapeyron relationship, and from the fact that models indicate that relative humidity would remain nearly constant. Under increased specific humidity and given that precipitating systems exhibit a tendency for feeding mostly on the moisture present in the atmosphere rather than on evapotranspiration (Trenberth 1998, 1999b), average precipitation increase as well as more intense rainfall events are thus to be expected and climate extremes are likely to be more frequent in the future (Christensen et al. 2007). On the other hand, an overall decrease in intensity of lower rainfall events and/or a decrease in frequency of all rainfall events is also projected (Trenberth et al. 2003).

Locally many factors could influence the global evolution of the precipitation pattern, such as changes in the main oscillation modes of the climate system, changes in the location and intensity of storm tracks or a modification of the vertical temperature profile induced by the radiative effects of greenhouse gases. Regional climate modelling offers the potential for addressing the local specificities of the projected evolution of the hydrological cycle.

Indeed, considering that hydrological processes strongly rely on surface processes, topography and atmospheric mesoscale circulations, their representation can be expected to improve with higher resolution (Iorio et al. 2004). Yet this is not straightforward as pointed out by Giorgi and Marinucci (1996) who showed that sensitivity of subgrid-scale parameterizations to spatial resolution could cancel the benefits of higher resolution unless the parameterizations are suitably adapted.

The potential added value of Regional Climate Models (RCM) can thus be defined as their ability to simulate finer scale details while reproducing correctly the large-scale fields provided by the driving Global Climate Models (GCM) or global analyses. The added value of RCMs depends on several factors: the nesting technique, the quality of lateral boundary conditions, the numerical discretization and truncation, the nonlinear interactions between different scales, the improved representation of topography and physiographic fields, and the performance of subgrid-scale parameterization. It is expected that the main RCM added value will be found in medium to fine scales that are poorly resolved, or even not resolved at all, by low-resolution GCMs (Laprise 2003).

A usual way of looking for RCM added value has been to focus on medium scales that are commonly resolved by both RCMs and GCMs, and to compare them to observations (e.g., Feser 2006). This permits to state objectively whether RCM fields have been improved relative to GCM ones. A second approach would be to consider the smaller scales that are resolved exclusively by RCMs, and to study their importance relative to larger scales (e.g., Van Tuyl and Errico 1989; Bielli and Laprise 2006, 2007). But these smaller scales cannot be compared to GCM-simulated fields and their comparison with high-resolution observations is often difficult. Should the smaller scales be found important, no more than the existence of potential added value could be concluded out of it. The present study will focus on the nonlinear interactions involving the medium and smaller scales in the atmospheric water budget as simulated by an RCM driven by a GCM.

A scale-decomposition tool is required to separate the scales of interest from the others. Spectral analysis as a scale-decomposition tool has been widely used with global models (Boer and Shepherd 1983; Boer 1994). However on limited-area domains, there is no rigorous way of applying spectral transforms to non-periodic fields (Laprise 2003). Yet several relatively successful attempts have been made so far and could legitimate the method (Boyd 2005). Errico (1985) proposed removing a linear trend from the fields to make them periodic before applying a Fourier transform; this trend has since then been defined differently by several authors. More recently Denis et al. (2002) used a discrete cosine transform (DCT) to spectrally analyze fields without subtracting any component; this is equivalent to assuming two-dimensional symmetry of the fields and applying a discrete Fourier transform to them.

Bielli and Laprise (2006) proposed a methodology to decompose the regional-scale atmospheric water budget into different spatial scales. They applied it to a simulation of a single winter month over North America with the Canadian Regional Climate Model (CRCM; Caya and Laprise 1999) driven by NCEP-NCAR reanalyses, and they focused their study on the time–mean budget. Bielli and Laprise (2007) generalized their previous results with a 25-year CRCM simulation (1975–1999) also driven by NCEP-NCAR reanalyses. They considered the winter and summer seasons and also analyzed the time variability of each term of the atmospheric water budget. The contribution of small scales appeared to be important, especially for the time variability of the fields.

The present study applies the methodology of Bielli and Laprise (2006, 2007) to two 30-year simulations over North America performed with the CRCM driven by the Canadian Coupled Global Climate Model (CGCM; McFarlane et al. 2005). The first simulation corresponds to the current climate (1961–1990), while the second corresponds to a future one (2041–2070) following the IPCC SRES A2 scenario (Nakicenovich et al. 2000). The present study aims: (1) to better understand the atmospheric water budget as simulated by an RCM, taking advantage of a scale-decomposition tool, (2) to investigate the changes in the atmospheric water budget that accompany a projected warmer climate, and also (3) to assess the potential added value of fine scales that are resolved in the CRCM but absent in the driving CGCM. Section 2 presents the experimental framework. Section 3 focuses on the current climate. Comparison will be made with the results of Bielli and Laprise (2007) in order to evaluate the sensitivity of the CRCM to different experimental configurations in simulating the current climate. It is important to note that only the methodology used here is similar to Bielli and Laprise's (2007) work. The driving data are different (NCEP-NCAR for them and CGCM for us). The CRCM version is also different. In particular, our version includes an up-to-date surface scheme, whereas their version used a simple bucket model. And the domain size is larger here than in their study. Section 4 addresses the evolution of the water budget terms in the future climate. Finally Sect. 5 summarizes the results and discusses future work.

2 Experimental framework

The simulations were performed with the CRCM (CRCM_4.2; see Music and Caya 2007 for CRCM_4 description), driven by the CGCM (CGCM_3.1; Scinocca and McFarlane 2004; McFarlane et al. 2005).

2.1 The CRCM and CGCM models

The CRCM is a limited-area nested model based on the fully elastic non-hydrostatic Euler equations, solved with a semi-implicit semi-Lagrangian scheme. CRCM atmospheric variables are discretized in the horizontal on an Arakawa C-type staggered grid (Arakawa and Lamb 1977), on a polar-stereographic projection. A complete description of the dynamical formulation of the CRCM can be found in Bergeron et al. (1994), Caya and Laprise (1999) and Laprise et al. (1997). For this experiment the model was run with a 45-km grid mesh (true a 60 N), a 15-min timestep and 29 Gal-Chen terrain-following levels in the vertical (Gal-Chen and Somerville 1975) with a top computational level at 29 km. The lateral boundary conditions are provided through a one-way nesting method inspired of Davies (1976) and refined by Yakimiw and Robert (1990). For this experiment the nesting data were provided by the CGCM. The nested variables are sea-level pressure, the horizontal wind components, humidity and temperature. Orography, soil and vegetation properties are prescribed, and sea-surface temperature and sea-ice are defined by interpolating the CGCM-simulated fields. On the edges of the domain a 9-grid point sponge zone is applied to gradually relax the wind components to the driving data. A spectral nudging technique of large-scale winds is also applied (Riette and Caya 2002). The physical parameterization package is mostly based on the CGCM_3.1 (Scinocca and McFarlane 2004), except for moist convection that follows Bechtold–Kain–Fritsch's parameterization (Kain and Fritsch 1990; Paquin and Caya 2000; Bechtold et al. 2001). In particular, the CRCM uses the Canadian Land-Surface Scheme (CLASS; Verseghy 1991; Verseghy et al. 1993). It is a three-layer soil model, which also includes a snow layer where applicable, and a vegetative canopy treatment. Its prognostic variables are frozen and liquid soil moisture content as well as temperature, which evolve following energy and moisture fluxes at the top and bottom of each layer. Fluxes are computed according to Darcy's equation. Soil surface properties are taken to be functions of the soil and vegetation types and soil moisture conditions within a given grid volume.

The CGCM is a spectral model with a 47-wave triangularly truncated spherical harmonic expansion in the horizontal. This corresponds to a minimal equatorial wavelength of 850 km (e.g., Laprise 1992). The vertical representation is in terms of rectangular finite elements defined on a hybrid vertical coordinate, as described by Laprise and Girard (1990). In the vertical, 32 levels span from the surface to approximately 50-km height. A description of the atmospheric and ocean components can be found in McFarlane et al. (2005) and Flato and Boer (2001), respectively.

2.2 The CRCM simulations

The current climate simulation was performed following the observed greenhouse and aerosols distributions, while the future climate one followed the IPCC SRES A2 scenario (Nakicenovich et al. 2000). The RCM simulations

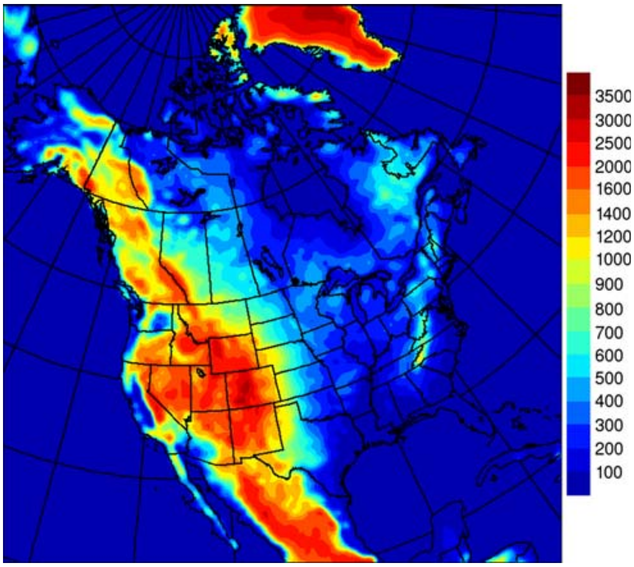

Fig. 1 Topographic height over the domain used for diagnostics (m)

were started for forcing conditions corresponding to 1 January 1958 and 1 January 2038, respectively. Both simulations were run for 33 years; the first 3 years were discarded as spin-up period, and the diagnostics were performed for the periods 1961–1990 and 2041–2070, respectively. Both simulations were driven by the CGCM atmospheric fields that were archived every 6 h and linearly interpolated in time at the CRCM time steps (15 min). Sea surface temperature and sea ice were interpolated from daily CGCM values to the CRCM time steps. Spectral nudging was applied to horizontal winds with length scales larger than 1,400 km, with increasing strength with height, starting just above 500 hPa and reaching a characteristic relaxation time of 10 h at the model top ($\sim$10 hPa). The regional domain, centred over Canada, contains 200 by 192 grid points. In the following, all fields will be analysed on a 172 by 172 grid-point central domain (the square domain facilitating the Fourier transform application). Figure 1 represents the model topography over that domain.

2.3 Methodology

The methodology employed follows that of Bielli and Laprise (2006, 2007). Let us consider the vertically integrated atmospheric water budget as defined by Peixoto and Oort (1992):

$$\partial_t \bar{q} = -\nabla \cdot \bar{\mathbf{Q}} + E - P,$$

where q is the specific humidity, $\mathbf{Q} = \mathbf{V}q$ the horizontal atmospheric water vapour flux, E the surface evapotranspiration, P the precipitation reaching the surface, and the overbar represents the mass-weighted vertical integration. In the following, each of the four terms of the water budget equation will be presented in units of millimeters per day.

The model-simulated variables were archived at six hourly intervals on Gal-Chen levels. Precipitation and evapotranspiration amounts were accumulated between archival times during the integration of the model. The moisture flux $\mathbf{Q} = \mathbf{V}q$ was vertically integrated on Gal-Chen levels at each time step during the integration of the model, and also accumulated between archival times. The time- and vertically-integrated moisture flux divergence $\nabla \cdot \bar{\mathbf{Q}}$ was then calculated with centred finite differences at each archival time. Finally specific humidity was sampled and vertically integrated at each archival time, and the vertically integrated water vapour tendency $\partial_t \bar{q}$ was evaluated as a finite difference between two instantaneous archival data.

Moreover in order to decompose the moisture flux divergence into interaction terms of wind and humidity, the horizontal wind and specific humidity instantaneous fields, $\mathbf{V}$ and q, were also sampled every 6 h and interpolated on 30 pressure levels in the vertical. This was a necessary step in order to proceed with the scale decomposition on quasi-horizontal pressure surfaces rather than on Gal-Chen terrain-following levels. Then the moisture flux and its divergence were computed for various wave bands, and vertically integrated in pressure. We note that 23 of the 30 pressure levels were used below 700 hPa to have a good vertical resolution in the lower troposphere, where atmospheric water vapour is concentrated; Bielli and Laprise (2006) showed the importance of a sufficient vertical resolution in the lower troposphere to reduce interpolation errors.

2.3.1 *Scale decomposition*

Each variable X of the water budget (2D-fields), as well as the horizontal wind and humidity 3D-fields (on pressure levels), were decomposed into three spatial scales as follows: $X = X_0 + X_L + X_S$. Here X_0 represents the very large scales that are resolved by the CGCM and transferred to the CRCM by the lateral driving; these were approximated as the domain-mean value. X_{L} represents the large scales resolved by both the CRCM and the driving CGCM. Finally X_{S} represents the small scales resolved exclusively by the CRCM. In the following, when presenting the scale-decomposed water budget variables, large and very large scales will always be gathered and called large scales for short. The scale decomposition was performed by using the DCT tool of Denis et al. (2002). Following Bielli and Laprise's (2006) choice, all scales larger than 1,000 km were kept in the large-scale term exclusively, and all scales smaller than 600 km were kept in the small-scale term exclusively, with a smooth transition as a cosine square in the intermediate range from 600 to 1,000 km to reduce Gibbs' effects. Considering the effective resolution of the driving spectral model as twice its equivalent equatorial grid spacing, which is defined in various ways by Laprise (1992), the effective resolution of the CGCM would reside roughly in the intermediate range from 600 to 1,000 km used here for the scale decomposition.

The three scales of horizontal winds and specific humidity were combined to provide nine interaction terms of the form

$$\mathbf{V_a} q_\mathbf{b}, \quad (\mathbf{a}, \mathbf{b}) \in (0, L, S) \tag{1}$$

Those terms were vertically integrated on pressure levels using a numerical quadrature as follows:

$$\overline{\mathbf{V_a} q_\mathbf{b}} = \frac{1}{g} \sum_{i=1}^{30} \beta^i \mathbf{V}_\mathbf{a}^i q_\mathbf{b}^i \Delta p_{1/2}^i$$

where the superscript i refers to the values of the fields at the ith pressure level and $\Delta p_{1/2}^i$ is the pressure thickness of the layer. In this summation, use was made of Boer's (1982) mask β in order to adequately account for topography while integrating on all pressure levels; this allows handling more easily statistics of fields interpolated on pressure levels.

Finally calculating the divergence of these terms with centred finite differences on the polar-stereographic grid provided the following decomposition of the total moisture flux divergence:

$$\nabla \cdot \bar{\mathbf{Q}} = (\nabla \cdot \bar{\mathbf{Q}})_R + (\nabla \cdot \bar{\mathbf{Q}})_U \tag{2}$$

with

$$(\nabla \cdot \bar{\mathbf{Q}})_R = \nabla \cdot \overline{\mathbf{V}_0 q_0} + \nabla \cdot \overline{\mathbf{V}_0 q_L} + \nabla \cdot \overline{\mathbf{V}_L q_0} + \nabla \cdot \overline{\mathbf{V}_L q_L} \tag{2a}$$

and

$$(\nabla \cdot \bar{\mathbf{Q}})_U = \nabla \cdot \overline{\mathbf{V}_0 q_S} + \nabla \cdot \overline{\mathbf{V}_S q_0} + \nabla \cdot \overline{\mathbf{V}_L q_S} + \nabla \cdot \overline{\mathbf{V}_S q_L} + \nabla \cdot \overline{\mathbf{V}_S q_S} \tag{2b}$$

In the following, the nine components will be referred to as the interaction terms. These nine terms contained in $\nabla \cdot \bar{\mathbf{Q}}$ will sometimes be gathered to form a CGCM-resolved term $(\nabla \cdot \bar{\mathbf{Q}})_R$ and a CGCM-unresolved term $(\nabla \cdot \bar{\mathbf{Q}})_U$. The CGCM-resolved term involves interactions of scales that are present in both the CRCM and the CGCM, while the CGCM-unresolved term involves interactions comprising at least one component whose scale is too small to be resolved by the CGCM. It is important to note that the product of any two scales will project on scales that are larger and smaller; therefore the CGCM-resolved and CGCM-unresolved terms should not be confused with large- and small-scale terms.

2.3.2 Statistics

The diagnostics fields were computed for the simulated winter (DJF) and summer (JJA) seasons by means of several statistics. Over North America, the water budget balance is expected to differ markedly between seasons due to more vigorous mid-latitude synoptic systems in winter and more convection in summer. Let us denote by $X_{j,y}$ the archive of variable X, where the subscript j refers to the time step within the season and y refers to the year, and by $X_y^J = \frac{1}{J}\sum_{j=1}^{J} X_{j,y}$ its seasonal average for year y, with J the number of time steps within a season. With Y representing the number of years analyzed, we can then define the following climatological statistics:

- the seasonal mean

$$X^{J,Y} = \frac{1}{Y \cdot J} \sum_{y=1}^{Y} \sum_{j=1}^{J} X_{j,y},$$

- the total seasonal variance

$$\sigma_c^2 = \frac{1}{Y \cdot J} \sum_{y=1}^{Y} \sum_{j=1}^{J} \left(X_{j,y} - X^{J,Y}\right)^2,$$

- the intraseasonal variance

$$\sigma_{cis}^2 = \frac{1}{Y \cdot J} \sum_{y=1}^{Y} \sum_{j=1}^{J} \left(X_{j,y} - X_y^J\right)^2,$$

- the interannual seasonal variance

$$\sigma_{ias}^2 = \frac{1}{Y} \sum_{y=1}^{Y} \left(X_y^J - X^{J,Y}\right)^2,$$

such that

$$\sigma_c^2 = \sigma_{cis}^2 + \sigma_{ias}^2 \tag{3}$$

Moreover, when combining spatial and temporal decompositions, covariance terms arise in the calculation of temporal variability. For example, if we consider the field $X = X_L + X_S$ decomposed in terms of its large-scale X_L and small-scale X_S components, any of its variances can be expressed as

$$\sigma_c^2(X) = \sigma_c^2(X_L) + \sigma_c^2(X_S) + \mathrm{cov}(X_L, X_S) \tag{4}$$

Small scales appear in the sum $\sigma_c^2(X_S) + \mathrm{cov}(X_L, X_S)$, which represents the "potential added value" of the RCM in the time variability relative to the coarser-resolution driving model. In the following, the small-scale variance and covariance between large and small scales will always be presented together and referred to as the small-scale contribution for short. The same could also be applied to the case of the recomposed moisture flux divergence

$X = X_R + X_U$, for a CGCM-resolved term X_R and a CGCM-unresolved term X_U.

Finally, the local statistical significance level of climate-change projections has been checked for all variables investigated, according to the bootstrapping technique (Efron and Tibshirani 1993). This test has been carried out at each grid point both for the difference of climatological mean between future and current climates, and for the difference of intraseasonnal variabilities, in a two-sided configuration. In the climate-change section, only statistically significant values, according to a 5% rejection level, will be displayed. Note that a *t*-test has also been performed; it gave results very similar to those of the bootstrapping test.

3 Current climate

3.1 Winter season

3.1.1 Climatology of the atmospheric water budget

Before proceeding with the scale decomposition, it is instructive to look at the climatology of the vertically integrated atmospheric water budget in the simulation (Fig. 2).

A balance is noted between the climatological mean (top row) of precipitation (first column), evapotranspiration (second column) and horizontal moisture flux convergence (fourth column). Precipitation and evapotranspiration present maxima over both eastern Pacific and western Atlantic Oceans, but they are weaker over the continent. Atmospheric water flux convergence essentially balances precipitation over the northern oceans and the coastal regions of North America, while its divergence over southern oceans balances the large evapotranspiration there. The water vapour tendency (third column) plays a negligible role; its negative sign reveals the contribution of the annual cycle during the winter period (DJF).

An inspection of variability for all variables shows that the climatological variability is dominated by the intraseasonal component, while the interannual variability is much smaller and its pattern follows that of the intraseasonal variability (not shown). In the following only fields of intraseasonal variability will be presented.

All variables but evapotranspiration present a large variability (bottom row), with standard deviations exceeding their mean. Oceanic maxima of variability indicate the regions of largest synoptic activity, while the variability is smaller inland. Precipitation and evapotranspiration present a smaller variability than the two other variables, and their variability patterns are similar to their mean patterns, which we believe results from the positive-definite nature of these variables.

The climatology of the water budget of this CGCM-driven simulation can be compared to that obtained by Bielli and Laprise (2007) for a simulation with an earlier version of the CRCM driven by reanalyses. The climatological mean of all variables are very similar in both

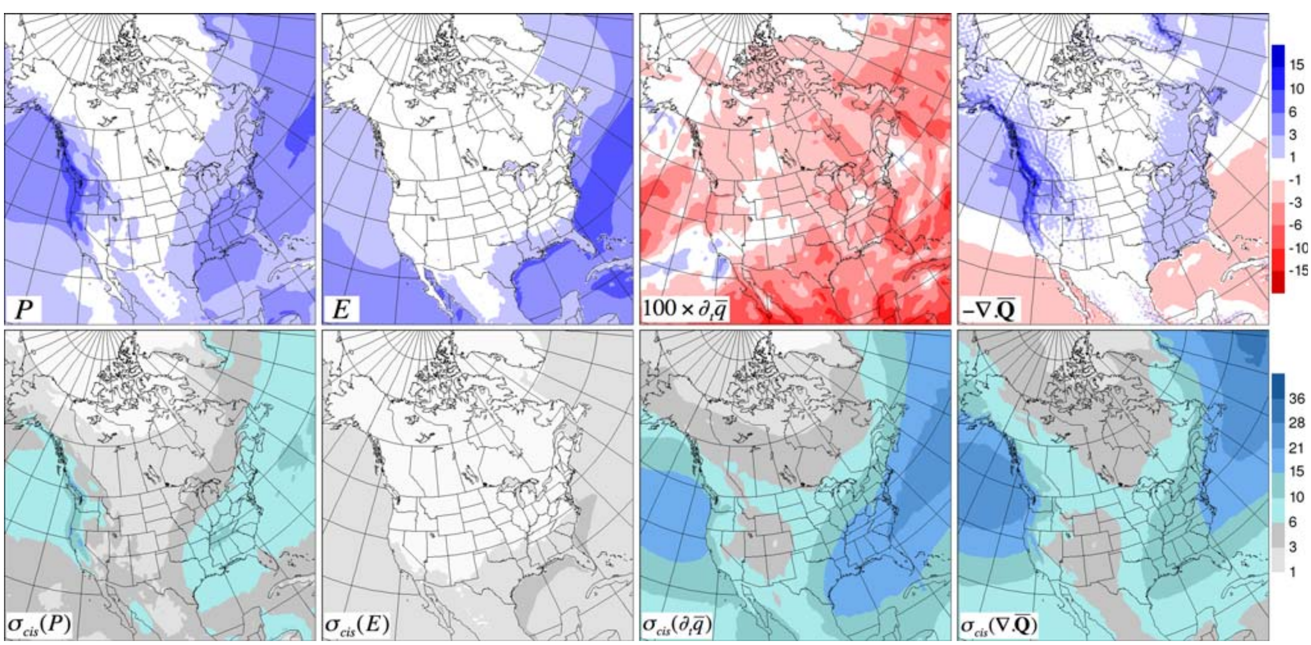

Fig. 2 Climatological mean (*top row*) and intraseasonal standard deviation (*bottom row*) of precipitation (*first column*), evapotranspiration (*second column*), vertically integrated water vapour tendency (*third column*) and vertically integrated atmospheric water flux convergence (*fourth column*), calculated from the CRCM simulation for the winter season from December 1960 to February 1990. Units are in mm/day. Note that the mean water vapour tendency has been multiplied by 100

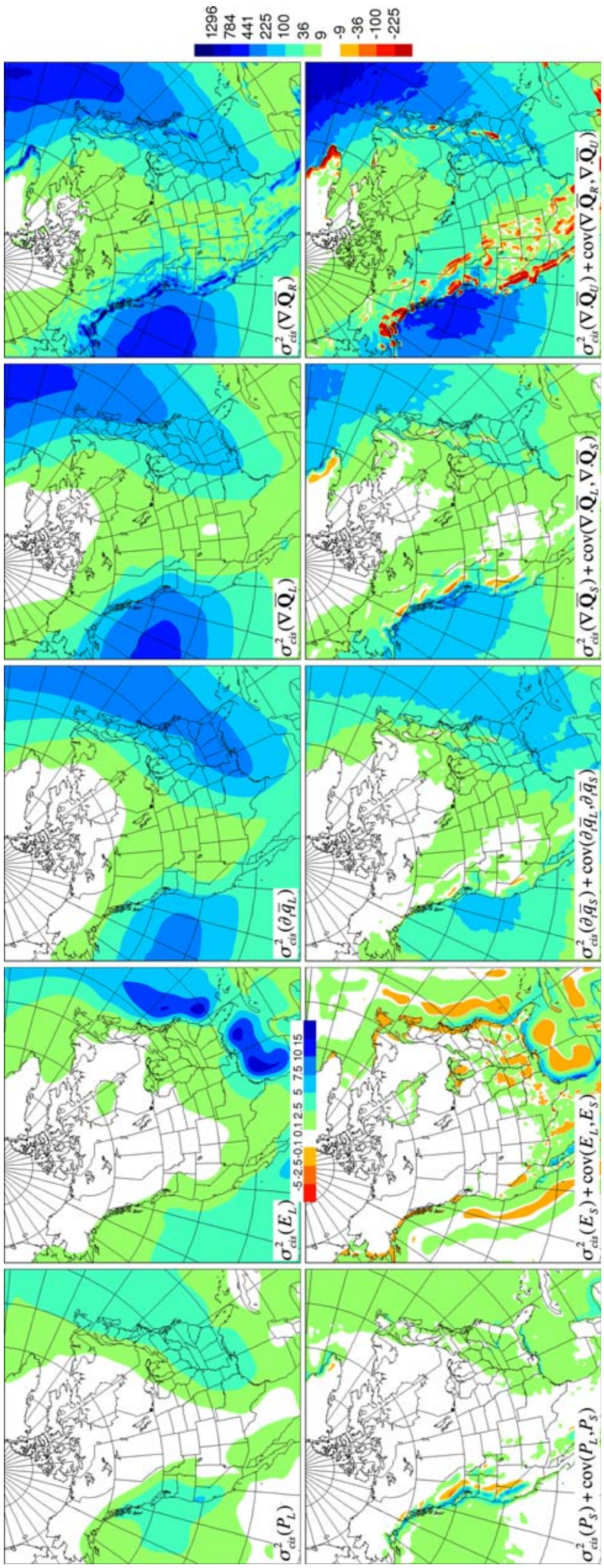

◀ **Fig. 3** First *four columns*: from left to right, climatological intraseasonal variance of the large-scale component (*top row*) and small-scale component plus covariance (*bottom row*) of precipitation, evapotranspiration, vertically integrated water vapour tendency and vertically integrated atmospheric water flux divergence. *Fifth column*: climatological intraseasonal variance of the CGCM-resolved term (*top panel*) and CGCM-unresolved term plus covariance (*bottom panel*), computed on pressure levels. All fields calculated from the CRCM simulation for the winter season from December 1960 to February 1990. Units are in mm^2/day^2. The scale is common to all *panels* except for evapotranspiration fields (*horizontal scale*)

simulations, in pattern and amplitude. The precipitation field is even slightly improved here: it reproduces the dry area observed over the central United States (see CRU observations in Fig. 3 of Bielli and Laprise 2007), which they failed to simulate. Time variability fields also exhibit very similar patterns in both simulations. However, our simulated fields display an overall slightly smaller variability except for the oceanic maxima of the atmospheric water flux divergence that are larger in our results. Precipitation variability remains nearly unchanged. The many differences between the configurations of our simulations and that of Bielli and Laprise (2007) (see Sect. 1) prevent us from assessing in any simple way the origins of these differences. However, for the same reason, this level of agreement illustrates the ability of the CRCM to simulate a reasonable climate under altered driving conditions.

3.1.2 Scale decomposition of the water budget terms

Bielli and Laprise (2006) have shown that the contribution of small scales to the climatological mean budget is quite modest, suggesting that large scales are mainly responsible for the maintenance of the time mean. The stationary small scales are confined near complex topographic features (for precipitation and water vapour flux divergence) or land-sea contrasts (for evapotranspiration), and they never exceed large scales in amplitude.

The contribution of small scales to time variability is much more important. The top row of Fig. 3 presents the intraseasonal variance of the large-scale component of the atmospheric water budget variables (first four columns) and the bottom row, that of the small-scale component. Unlike the other variables, the variability of evapotranspiration arises essentially from large scales, whereas small scales are confined along the coasts and contribute to better resolving a near-discontinuity at the shoreline. For the three other variables, small scales exhibit patterns very similar to the large-scale ones. While they remain overall smaller than large scales, small scales still represent a significant contribution to variability fields, and even exceed large scales locally, e.g., over the Caribbean and Arctic regions. These transient small scales largely cancel upon time averaging and are therefore not seen in the time-mean part; the contribution of the small-scale variability suggests a significant added value of transient small scales to the water budget climatology. Unlike stationary small scales that are linked to stationary forcings such as topography, transient small scales are rather related to mid-latitude synoptic systems along the storm tracks in winter.

3.1.3 Decomposed temporal variability of the moisture flux divergence

Taking advantage of the quadratic nature of the atmospheric water flux divergence, this term can also be decomposed into scale interactions by scale-decomposing the wind and humidity fields that enter it (Eq. 1). Regrouping these scale interactions into a CGCM-resolved component (R, Eq. 2a) and a CGCM-unresolved component (U, Eq. 2b) allows evaluating which part of this field can be resolved by both the low-resolution CGCM and the CRCM, and which part by the CRCM only. This is expected to give a better estimation of the added value of small scales than the projection of the total field onto large and small scales alone.

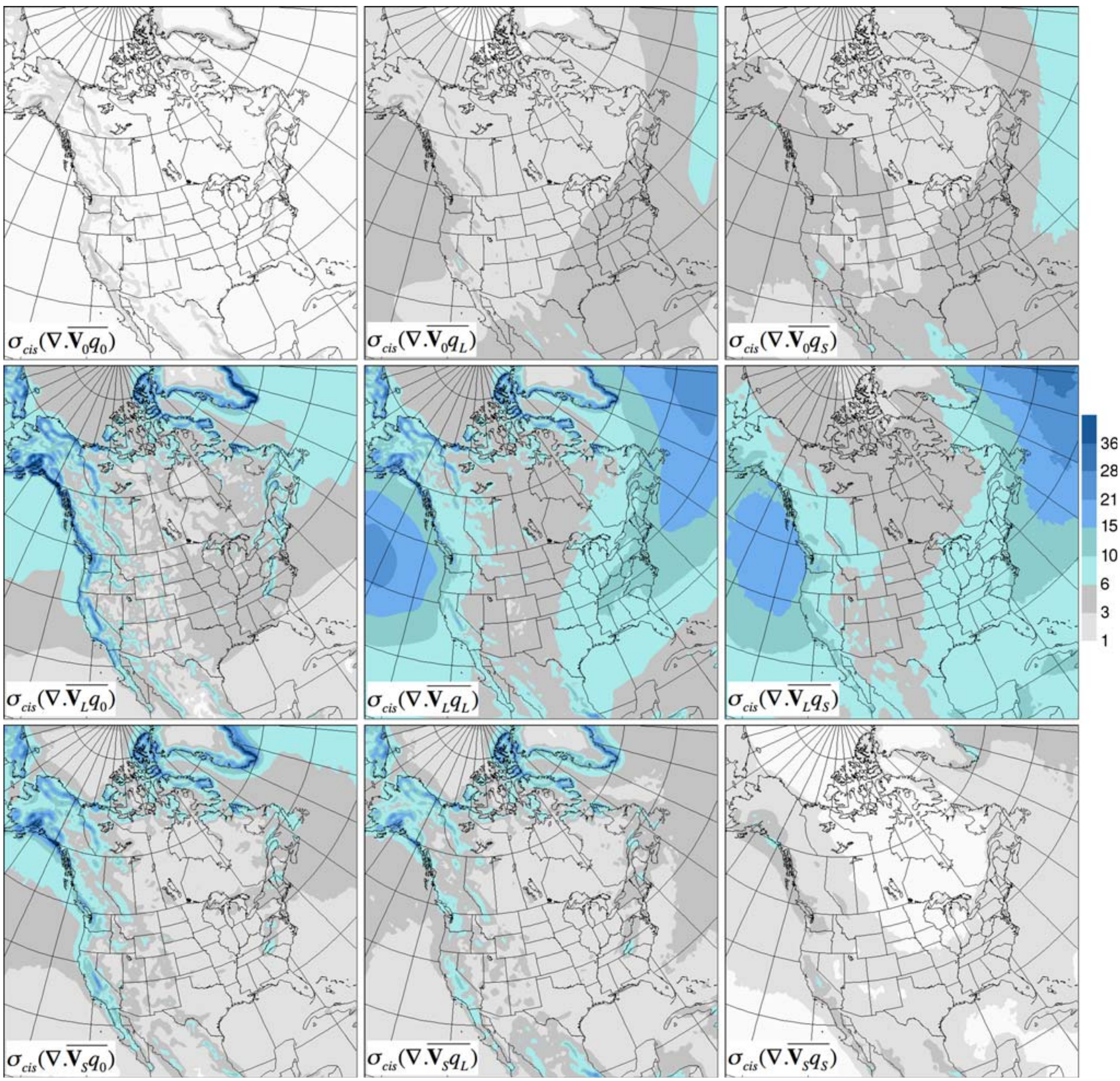

Fig. 4 Climatological intraseasonal standard deviation of the nine interaction terms entering the vertically integrated atmospheric water flux divergence, calculated on pressure levels from the CRCM simulation for the winter season from December 1960 to February 1990. Units are in mm/day

The fifth column of Fig. 3 shows the intraseasonal variance of R (top panel) and U (bottom panel). Both terms show similar patterns and appear equally important to time variability. Their amplitudes are comparable over the Pacific Ocean, R is larger over the eastern part of the continent, but U is larger over the northern Atlantic Ocean and even dominates over the Caribbean region and the north of the continent. This suggests a substantial potential added value of the CRCM which, unlike the CGCM, should be able to properly resolve the moisture flux divergence variability field in regions where U is important. Moreover, it seems that in some regions, such as over the northern Atlantic Ocean, part of the large-scale variability of the moisture flux divergence (Fig. 3, fourth column) results from interactions that are unresolved by the low-resolution CGCM. This illustrates how studying the scale interactions in a quadratic term besides the scale projections can lead to a better evaluation of the added value of small scales.

To gain a better insight into the contribution of each scale, Fig. 4 presents the intraseasonal standard deviation of each of the nine interaction terms (Eqs. 2a, 2b). The four upper left panels arise from interactions between large- and very large-scale terms and thus contribute to R, while the other five panels arise from interactions that involve at least one small-scale variable and thus contribute to U. Two terms, involving the large-scale wind, dominate: $\nabla \cdot \overline{\mathbf{V}_L q_L}$ contributing to R and $\nabla \cdot \overline{\mathbf{V}_L q_S}$ contributing to U. Interestingly, the former, involving the large-scale humidity, is larger over the Pacific Ocean, while the latter, involving the small-scale humidity, is larger over the northern Atlantic Ocean. We also note that all the terms involving the small scales of humidity present more variability over oceans, whereas those involving the small scales of wind display more variability over topographic features. This suggests different mechanisms producing small scales of wind and humidity: orographic for the former, and more related to synoptic activity for the latter.

3.2 Summer season

3.2.1 *Climatology of the atmospheric water budget*

Let us now turn to the simulated summer water budget climatology (Fig. 5). As in winter, a mean balance is achieved between precipitation, evapotranspiration and the atmospheric water flux convergence (top row). Variability (bottom row) is essentially intraseasonal, with an amplitude larger than the mean for all variables. But compared to winter, this climatology reflects the more convective conditions prevailing over the continent and the Caribbean region in summer, as well as a northward shift of the synoptic activity.

Mean precipitation and evapotranspiration are stronger than in winter over the continent and the Caribbean region, but they are weaker nearly everywhere else over the oceans. The atmospheric water flux convergence is reduced over the continent and eastern Pacific Ocean but enhanced everywhere else over the oceans, which results in a northward shift of the main moisture convergence region.

Precipitation and evapotranspiration summer variability differs from winter variability in ways that are very similar to those of their mean. The atmospheric water flux divergence and water vapour tendency show variability patterns

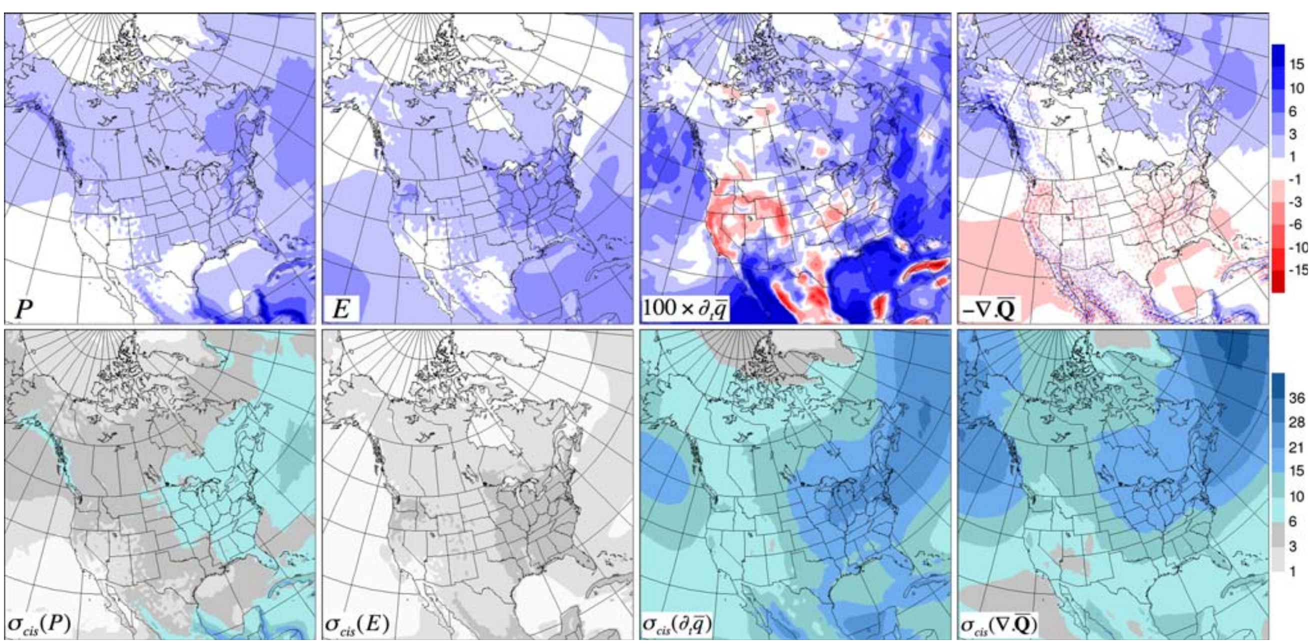

Fig. 5 Same as Fig. 2 but for the summer season from June 1961 to August 1990

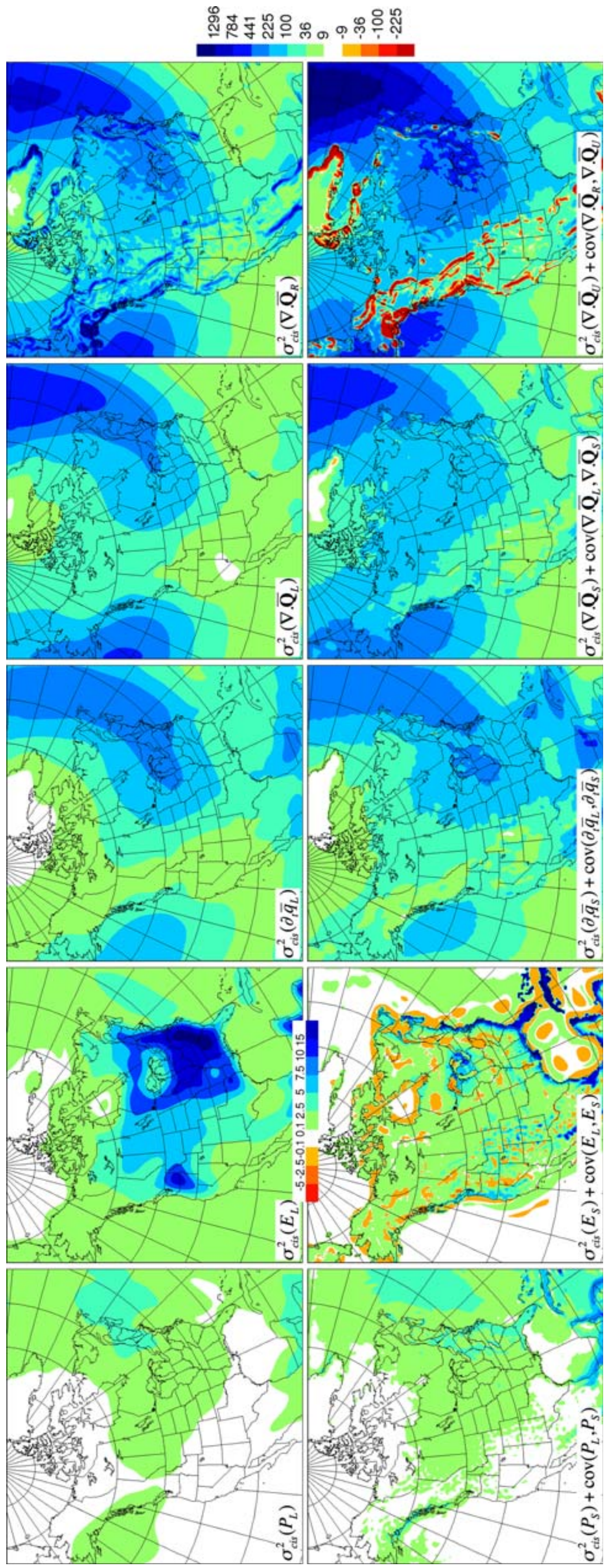

◀ **Fig. 6** Same as Fig. 3 but for the summer season from June 1961 to August 1990

quite similar to their winter ones but shifted to the north. Compared to winter their variability is clearly larger everywhere except over the eastern Pacific Ocean.

In summer more than in winter, large differences with the results of Bielli and Laprise (2007) are noted. Weaker mean precipitation, evapotranspiration and moisture flux convergence are noted in our results, especially over the eastern part of the continent, which makes our precipitation field closer to CRU observations (Fig. 10 of Bielli and Laprise 2007) than that of Bielli and Laprise (2007), which was overestimated. Time variability is clearly reduced over the continent for all variables, and especially over the eastern United States, compared to Bielli and Laprise's (2007) results. We believe that the use here of a more advanced and more comprehensive land-surface model, the Canadian Land Surface Scheme (CLASS; Verseghy 1991; Verseghy et al. 1993), instead of the original bucket model they used, might be the reason of our simulating a weaker, and improved, hydrological cycle over the continent (Music and Caya 2007).

3.2.2 *Scale decomposition of the water budget terms*

For all variables but evapotranspiration, both large and small scales present a summer variability overall larger than in winter everywhere but over the eastern Pacific Ocean (Fig. 6, first four columns). Contrary to winter the small-scale contribution is larger than the large-scale one nearly everywhere and even dominates over the Arctic, Caribbean and southwestern mountainous regions. These transient small scales are not only related to synoptic activity as in winter, but also to the strong summer continental convection. Large-scale variability remains larger over a region extending a few thousand km eastward from the Great Lakes, which corresponds to the location of the storm track as revealed by the 300-hPa meridional wind variability (not shown).

3.2.3 *Decomposed temporal variability of the moisture flux divergence*

Both R and U show a larger variability than in winter over the whole domain but the eastern Pacific Ocean, as well as a northward shift of their patterns (Fig. 6, fifth column). The importance of U is clearly enhanced in summer compared to winter: U clearly dominates R everywhere except over the Pacific Ocean. Moreover, as in winter, part of the large-scale variability, e.g., over the storm track-related band previously mentioned, appears to be ascribed to interactions unresolved by the low-resolution CGCM. Clearly the importance of correctly resolving small-scale interactions is enhanced in summer.

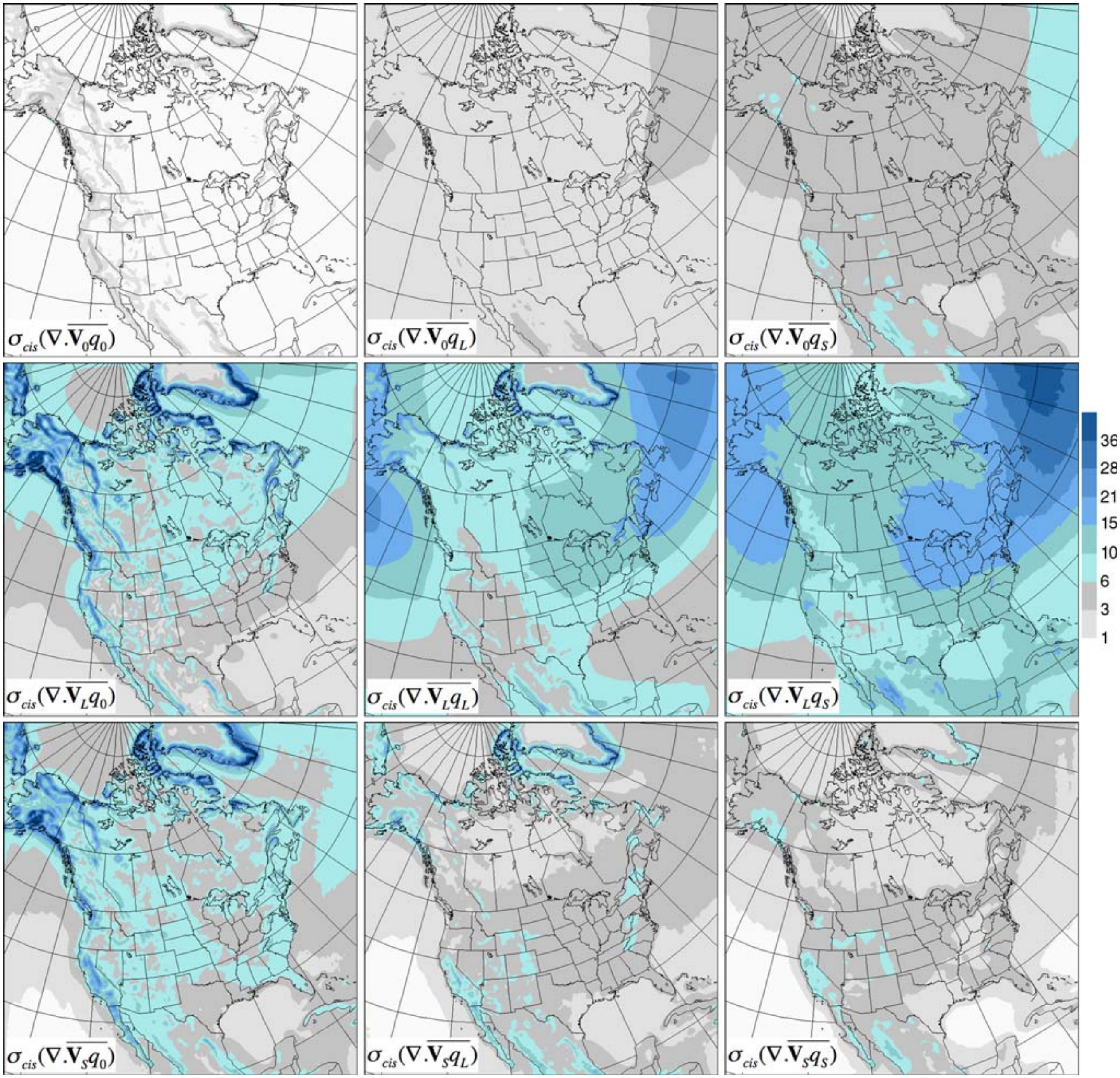

Fig. 7 Same as Fig. 4 but for the summer season from June 1961 to August 1990

Compared to winter, all the interaction terms in summer present a variability increase over the continent but a variability decrease over both oceans, especially the eastern Pacific Ocean (Fig. 7). While the same two interaction terms as in winter are responsible for most of the summer variability of R and U, i.e., $\nabla \cdot \overline{\mathbf{V}_L q_L}$ and $\nabla \cdot \overline{\mathbf{V}_L q_S}$, respectively, the relative increase in variability is clearly larger for terms contributing to U than for those contributing to R (not shown). The summer variability reaches more than three times its winter value for these terms.

4 Future climate

We now turn our attention to the future climate projection. In order to highlight the changes in the water budget variables, we will present fields of differences, either in the form of absolute difference "Future minus Current" simulated climates, or in the form of relative differences with respect to reference current-climate simulation. For all fields, only statistically significant values, according to a 95% confidence level, will be displayed and discussed.

4.1 Winter season

4.1.1 Climatology of the atmospheric water budget

Simulated fields in the future winters exhibit patterns similar to the current climate ones, but with a general intensification of the hydrological cycle.

The first three panels of Fig. 8 present the changes in the mean precipitation, evapotranspiration, and atmospheric water flux convergence; the fourth panel shows the relative change in precipitation. Precipitation exhibits a general increase over most of the domain, except the southernmost part. Overall precipitation changes seem closely related to similar changes in the atmospheric water flux convergence field, especially over the northern continent or the southern oceans. The precipitation zero-change line spreads approximately along the USA-Mexico border (within the region where changes are, almost by definition, not statistically significant), which is in fairly good agreement with the 21-model averaged mean precipitation change reported in the IPCC fourth Assessment Report (Christensen et al. 2007). Evapotranspiration is enhanced over most of the oceans, in particular over the western Atlantic Ocean, and to a lesser extent over the United-States. Its large decrease over the

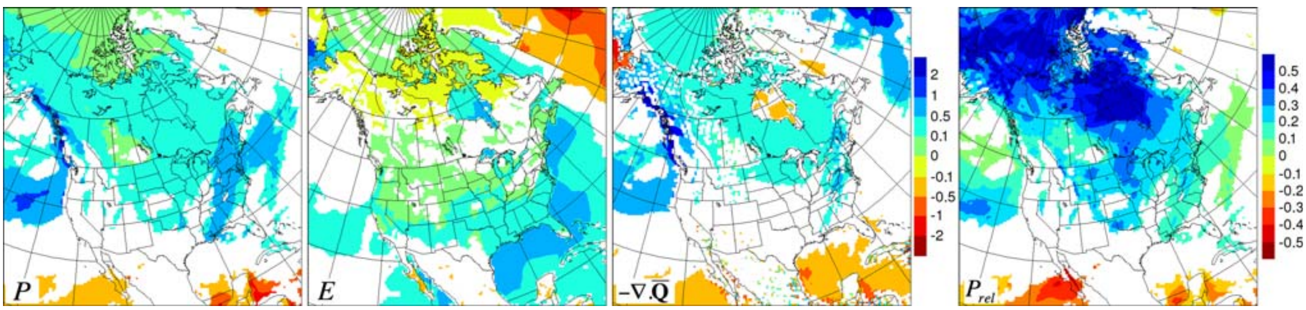

Fig. 8 Changes in the climatological mean of precipitation (*first panel*), evapotranspiration (*second panel*) and vertically integrated atmospheric water flux convergence (*third panel*), and relative changes in the mean precipitation (*fourth panel*), calculated from the CRCM simulation for the winter season from December 2040 to February 2070. Units are in mm/day. Note the different scale for relative changes

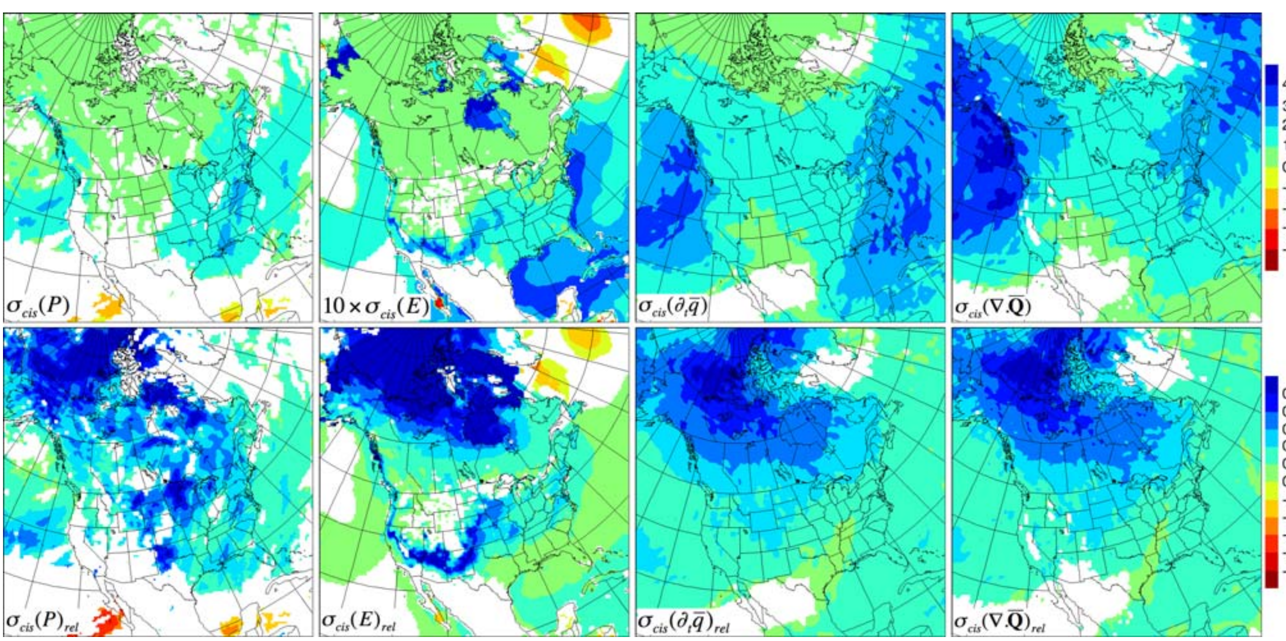

Fig. 9 Changes (*top row*) and relative changes (*bottom row*) in the climatological intraseasonal standard deviation of precipitation (*first column*), evapotranspiration (*second column*), vertically integrated water vapour tendency (*third column*) and vertically integrated atmospheric water flux divergence (*fourth column*), calculated from the CRCM simulation for the winter season from December 2040 to February 2070. Units in *top row panels* are in mm/day. Note that changes in the climatological intraseasonal standard deviation of evapotranspiration have been multiplied by 10

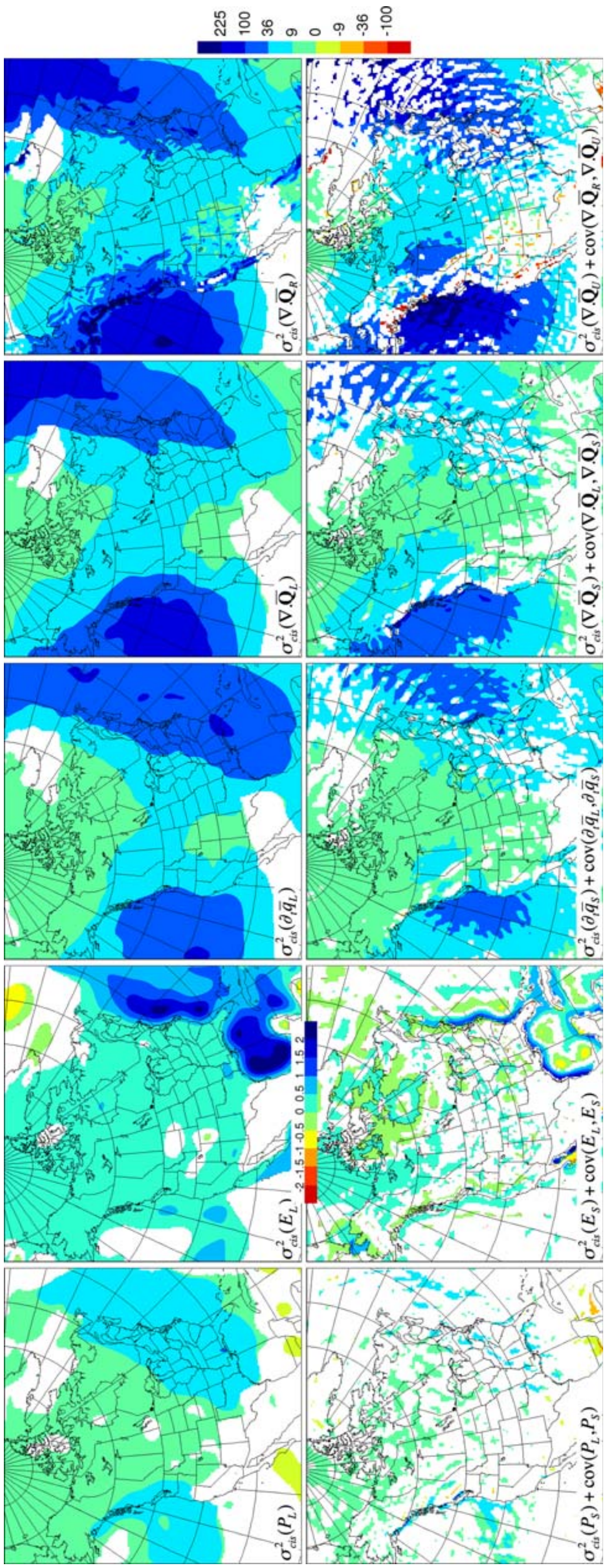

◀ **Fig. 10** First *four columns*: from left to right, changes in the climatological intraseasonal variance of the large-scale component (*top row*) and small-scale component plus covariance (*bottom row*) of precipitation, evapotranspiration, vertically integrated water vapour tendency and vertically integrated atmospheric water flux divergence. *Fifth column*: changes in the climatological intraseasonal variance of the CGCM-resolved term (*top panel*) and CGCM-unresolved term plus covariance (*bottom panel*), computed on pressure levels. All fields calculated from the CRCM simulation for the winter season from December 2040 to February 2070. Units are in mm^2/day^2. The scale is common to all *panels* except for evapotranspiration fields (*horizontal scale*)

northern Atlantic Ocean is partly balanced by a large increase in moisture convergence there. While only small absolute changes in precipitation and evapotranspiration are noted over the cold and dry Arctic region and north of the continent, for precipitation this corresponds nevertheless to a substantial relative increase exceeding 30% (fourth panel; idem but not shown for evapotranspiration).

Figure 9 shows the actual (top row) and relative (bottom row) changes in variability for the atmospheric water budget variables. It depicts a general increase in variability for all variables and over most of the domain; the only significant decreases occur over the northern Atlantic Ocean for evapotranspiration and over the southernmost part of the domain for precipitation. Actual changes are consistent in pattern with the present winter variability fields and their amplitude scales with that of the current climate variability (Fig. 2). Relative variability changes (bottom row) are comparable for all variables. As for the mean fields, they are maximal over the cold and dry northern regions, where they overall exceed 30% and locally reach 50%. These relative variability changes appear comparable with, but not significantly larger than, the relative mean changes.

4.1.2 Scale decomposition of the water budget terms

Unsurprisingly, the contribution of small scales to the future mean atmospheric water budget remains as limited as their contribution to the current time mean (not shown). However, their contribution to time variability changes is important. Figure 10 shows the changes in the intraseasonal variance of the large-scale (top row) and small-scale (bottom row) components of the atmospheric water budget variables (first four columns; the fifth column will be discussed in the next subsection). Both large- and small-scale components present an overall variability increase. Change patterns are consistent with current variability patterns, with largest changes associated to largest variability regions and variables. Large-scale changes are larger than small-scale changes nearly everywhere, and they dominate over both oceans, which is again consistent with their respective contributions to current variability fields. Largest relative changes occur over northern regions for both components (not shown). Relative changes are overall

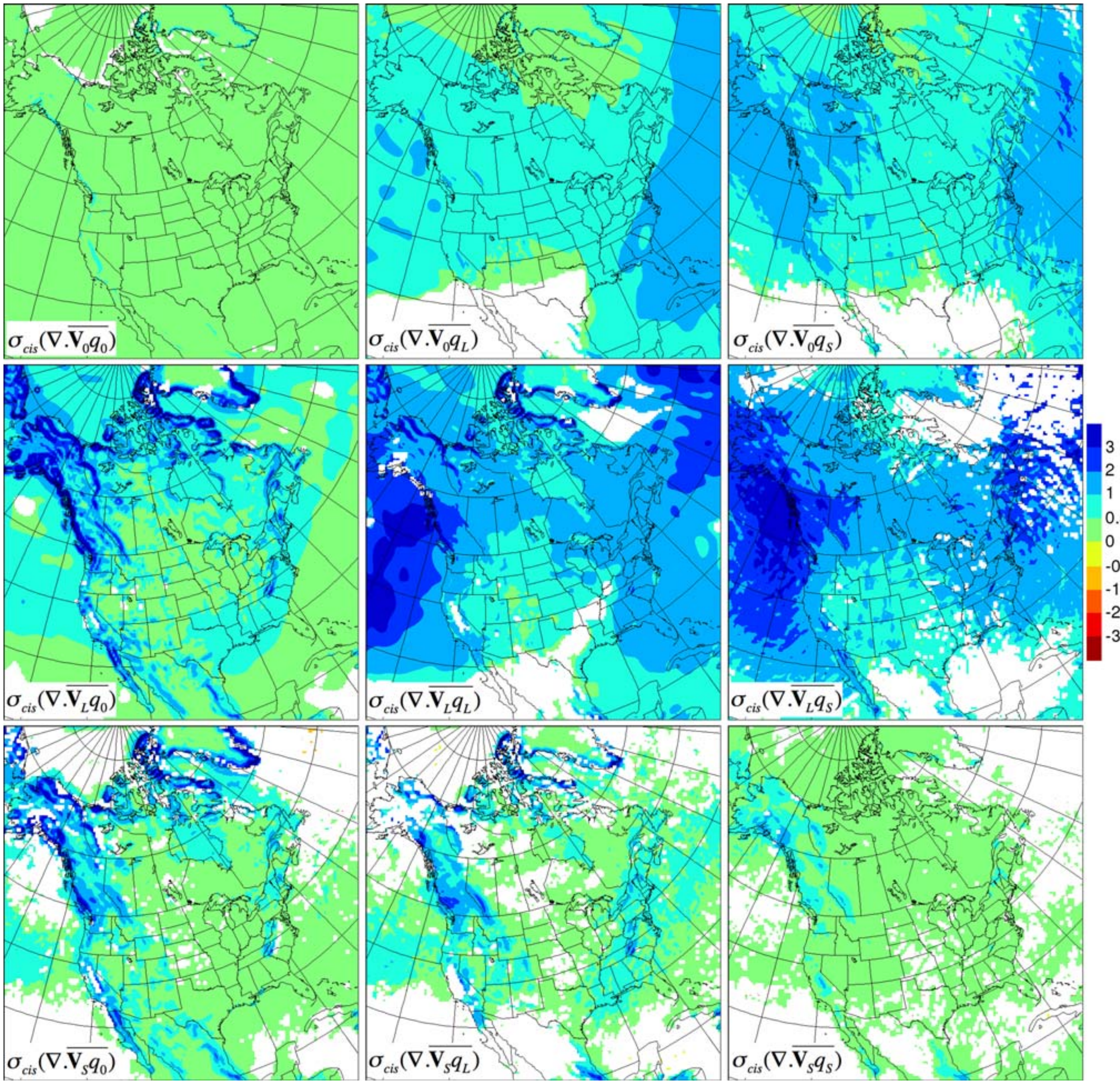

Fig. 11 Changes in the climatological intraseasonal standard deviation of the nine interaction terms entering the vertically integrated atmospheric water flux divergence, calculated on pressure levels from the CRCM simulation for the winter season from December 2040 to February 2070

larger for scales showing a smaller variability in the current climate, e.g., for small scales over the continent and both oceans dominated by synoptic activity, and for large scales over the Caribbean and Arctic regions. Statistically significant small scales of precipitation and evapotranspiration are very limited compared to those of the two other variables; this probably comes from their smaller amplitude, which might turn physically significant fields to statistically insignificant signals.

4.1.3 Decomposed temporal variability of the moisture flux divergence

The R and U contributions to the time variability of the moisture flux divergence (Fig. 10, fifth column, top and bottom panels, respectively) also present similar variability change patterns that are consistent with the current climate variability. Apart from the eastern Pacific Ocean, the increase in variability is overall larger for U than for R

everywhere, and in particular over the northern regions, but not over the Caribbean region, where changes are larger for *R*. This is rather unexpected since the Caribbean region was dominated by *U* in the current climate. Consequently, relative variability changes are larger for *R* than for *U* over the Caribbean region, but they are clearly larger for *U* than for *R* over the eastern continent and western Atlantic Ocean (not shown). In any case, largest relative changes remain located over the northern regions for both components (not shown).

All the interaction terms (Fig. 11) present an increased variability everywhere, with changes overall proportional to the amount of variability displayed in the current climate. Thus terms $\nabla \cdot \overline{\mathbf{V}_L q_L}$ and $\nabla \cdot \overline{\mathbf{V}_L q_S}$ still present largest changes. Interestingly, while terms involving the very large scales of wind or humidity presented comparable amounts of variability in the current climate, the variability increase seems larger for the former than for the latter. An inspection of relative variability changes (not shown) reveals that all terms present an increase above 10% and exceeding 20% over significant areas. Interestingly, the largest relative variability increase occurs for terms involving either the very large scales of wind or the small scales of humidity, and it is located over northern regions. This could be linked to stronger synoptic mid-latitude systems in the future winters favouring these particular scales (Christensen et al. 2007).

4.2 Summer season

4.2.1 Climatology of the atmospheric water budget

Contrary to winter, the summer atmospheric hydrological cycle does not undergo a general intensification. Time mean (Fig. 12) and time variability (Fig. 13) changes rather show an smaller intensification to the north, and a clear attenuation over a large southern part of the domain.

The increase in precipitation is confined to northern regions, while its decrease spreads over southern regions

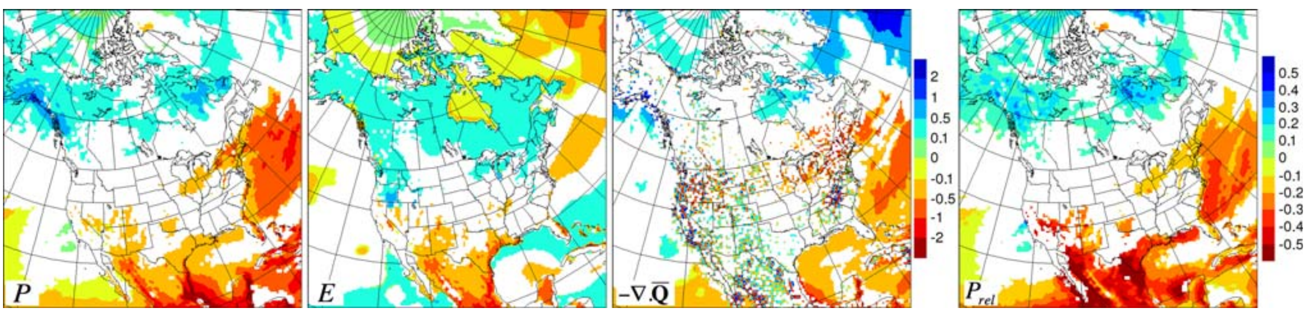

Fig. 12 Same as Fig. 8 but for the summer season from June 2041 to August 2070

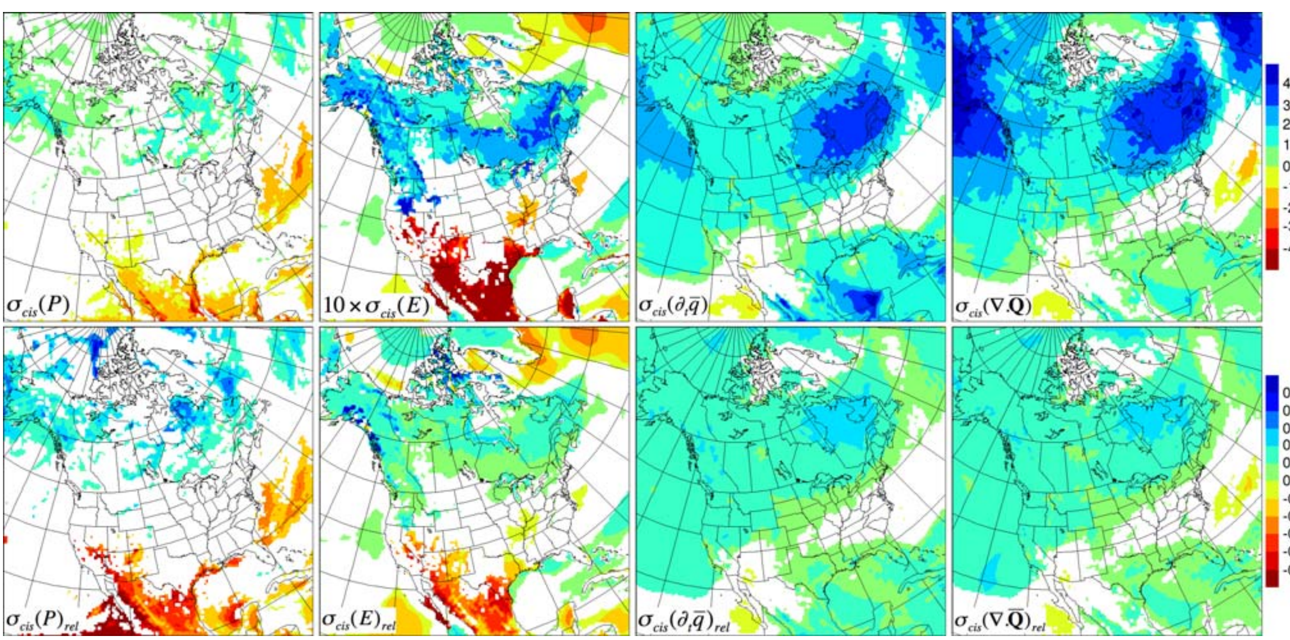

Fig. 13 Same as Fig. 9 but for the summer season from June 2041 to August 2070

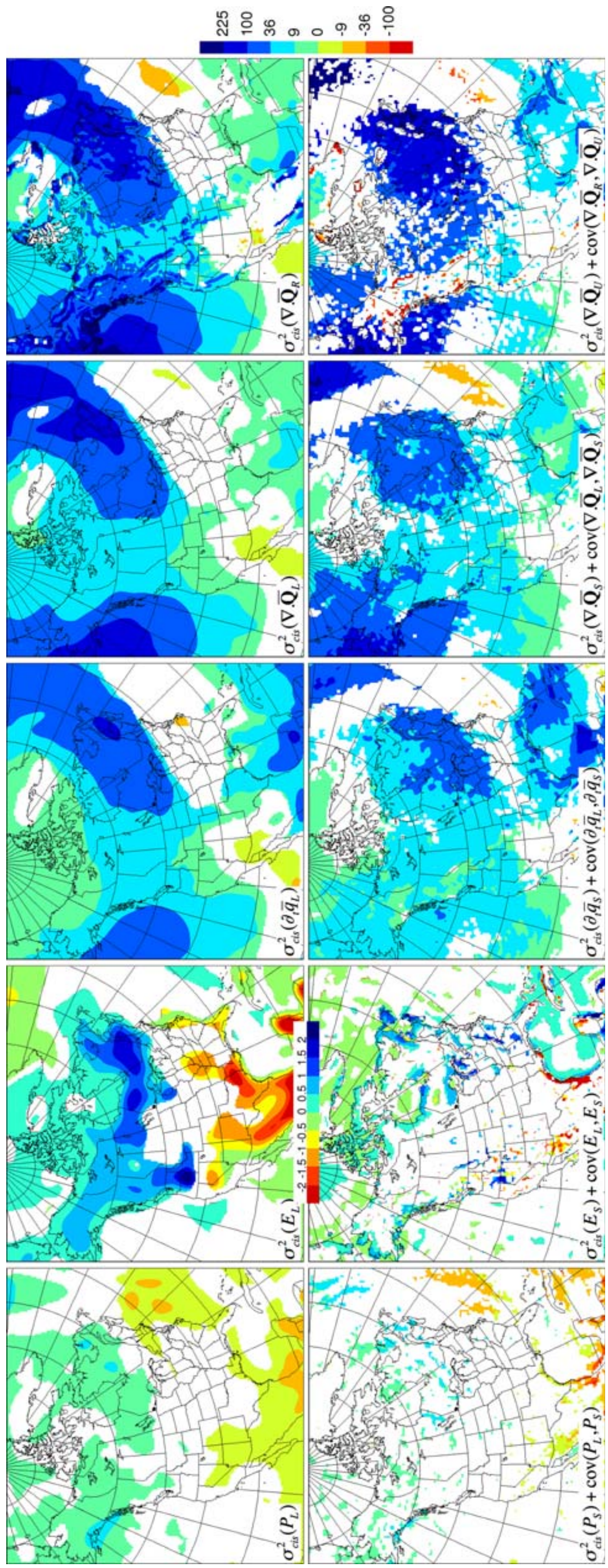

◀ **Fig. 14** Same as Fig. 10 but for the summer season from June 2041 to August 2070

and the western Atlantic Ocean (Fig. 12). In relative terms, this increase is smaller than in winter, while the decrease is much larger. The precipitation zero-change region lies approximately along the Canada–USA border (within the region where changes are not statistically significant), which is in fairly good agreement with the 21-model mean reported in the fourth Assessment Report of the IPCC (Christensen et al. 2007). Changes in precipitation appear to result more from similar changes in the atmospheric water flux convergence over oceans, and from similar changes in evapotranspiration over the continent. Compared to winter, the simulated summer changes in evapotranspiration are more pronounced over the continent but they are overall smaller over oceans. The reduction of evapotranspiration over the northern Atlantic Ocean remains important and is balanced by an enhanced moisture convergence there.

Time variability changes for precipitation and evapotranspiration show patterns similar to those of their mean changes (Fig. 13), with an increased variability over northern regions, and a decreased variability over southern regions, as well as the western Atlantic Ocean for precipitation and northern Atlantic Ocean for evapotranspiration. Unlike the two other variables, atmospheric water flux divergence and water vapour tendency still show an overall increase in variability, slightly larger than in winter, and maximal in relative terms over the northeastern Canada. The results also suggest variability decreases over the southwest of the domain and the western Atlantic Ocean for these variables. Contrary to winter, relative variability changes are similar in pattern to actual changes. The summer relative increases in variability are clearly smaller than in winter for every variable, whereas the relative decreases in variability cover a larger area. Relative variability changes also appear slightly smaller in amplitude than relative changes in the mean.

4.2.2 *Scale decomposition of the water budget terms*

Consistently with the current climate climatology, the contribution of small scales to summer variability changes is larger than in winter (Fig. 14). As in winter, statistically significant small scales of precipitation and evapotranspiration are very limited; however they support large-scale changes, and even exceed them locally, e.g. over the western Atlantic Ocean for precipitation. For the atmospheric water flux divergence and water vapour tendency, large-scale changes are larger over the Pacific Ocean and the storm track-related region extending eastward from the Great Lakes, which are the regions of mostly large-scale variability in the current climate. But small-scale changes clearly dominate over the Arctic and Caribbean regions, as well as over part of the continent, which is

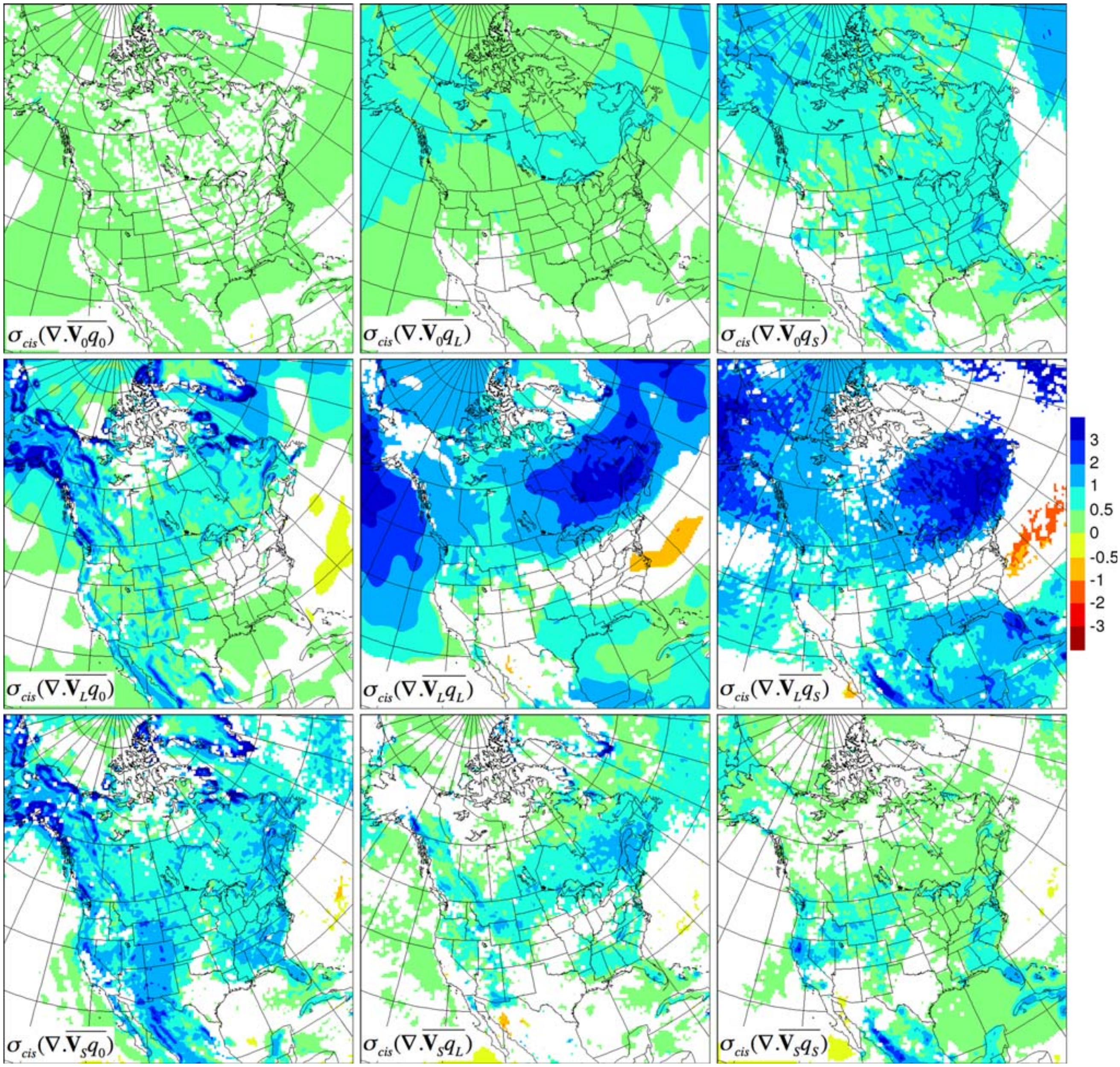

Fig. 15 Same as Fig. 11 but for the summer season from June 2041 to August 2070

again consistent with the current climate small-scale variability pattern. Variability decreases in the southwest of the domain and over the western Atlantic Ocean arise from both small- and large-scale components. Interestingly, relative changes are overall larger for large scales over the northern part of the domain and for small scales over the southeastern part of the domain (not shown). This could be linked to mid-latitude synoptic systems shifting to the north favouring more large scales, and more convection occurring in the southeast of the domain favouring more small scales.

4.2.3 *Decomposed temporal variability of the moisture flux divergence*

While both R and U components of the moisture flux divergence exhibit an overall increased variability (Fig. 14, fifth column), this increase is much larger for U than for R everywhere but over the eastern Pacific Ocean. Moreover, as noted for the large- and small-scale components of moisture flux divergence (Sect. 4.2.2), relative changes in R are larger to the north, whereas changes in U tend to be larger to the southeast of the domain (not shown).

Decreases in variability over the western Atlantic Ocean and the southwestern part of the domain seem more pronounced for R than for U.

As in winter, the largest summer variability changes are clearly those arising from the terms $\nabla \cdot \overline{\mathbf{V}_L q_L}$ and $\nabla \cdot \overline{\mathbf{V}_L q_S}$ (Fig. 15); however, summer relative changes are comparable for most of the interaction terms (not shown). Nevertheless, terms involving the very large scales of wind show a slightly larger relative variability increase located over the north of the continent, and terms involving the small scales of humidity present a larger relative increase over the Caribbean region than the other terms (not shown). Moreover, the western Atlantic decrease in variability seems to arise more from terms involving large scales of wind, while the southwestern decrease concerns more the small scales of wind. Compared to winter, summer variability changes appear to be larger for terms involving the small-scale wind and smaller for terms involving the large-scale wind. However relative changes are smaller than the winter ones for all the interaction terms (not shown).

5 Summary and conclusion

This paper investigated the scale-decomposed atmospheric water budget in the current climate (1961–1990) and in a projected warmer one (2041–2070) under SRES A2 scenario for winter and summer seasons, as simulated by the CRCM driven by the CGCM over North America.

Use was made of the decomposition tool of Denis et al. (2002) to decompose the water budget variables into three scales: very large scales, resolved by the CGCM and transferred to the CRCM by the lateral driving, large scales, resolved by both the CRCM and driving CGCM, and small scales that were resolved exclusively by the CRCM. In addition, the atmospheric water flux divergence was alternatively decomposed into nine interaction terms, involving the three scales of wind and humidity, and those interaction terms were gathered back to form a CGCM-resolved term and a CGCM-unresolved term. Finally, these scale-decomposed variables were decomposed into their time-mean and time-variability parts, and their seasonal statistics computed.

The contribution of each scale to the atmospheric water budget climatology, as well as to its change in a warmer climate, was investigated and the issue of potential added value of small scales that cannot be resolved by low-resolution CGCM, was addressed. The local statistical significance of the projected climate was also tested for every field investigated.

Results for the current climate appeared in fairly good agreement with those previously obtained by Bielli and Laprise (2007), despite some differences in the water budget climatology, especially in summer. The many differences between the regional model version and the configurations of our simulation and that of Bielli and Laprise (2007) prevented us from assessing in any simple way the origins of these differences, but at the same time they illustrated the ability of the CRCM to simulate a reasonable climate under altered driving conditions.

The atmospheric hydrological cycle appeared to be much more active over oceans than over land in winter, in relation to a strong synoptic activity there, while in summer a large contribution came from continental convection and synoptic activity seemed shifted to the north.

The intraseasonnal variability was found larger than the time mean for all variables, which highlights the importance of properly resolving the water budget variability. The scale decomposition showed that the contribution of small scales to time variability was significant for all variables but evapotranspiration in both seasons, and even dominant in summer. The contribution of the CGCM-unresolved component to the time variability of moisture flux divergence was also dominant, locally in winter, and nearly everywhere in summer, compared to the CGCM-resolved component. The finding that part of the large-scale variability could be ascribed to interactions involving small scales that cannot be resolved by the low-resolution CGCM illustrates the interest of studying scale interactions in nonlinear terms, besides the scale decomposition of total fields, in the search for added value in small scales.

Finally, the inspection of all interaction terms separately confirmed the previous results from Bielli and Laprise (2007), with two terms being responsible for most of the total variability of moisture flux divergence.

In the projection of future climate, water budget variables presented patterns similar to those of the current climate but exhibited an overall intensification of the hydrological cycle in winter, and an intensification to the north but a significant attenuation to the south in summer. In relative terms, changes were also larger in winter than in summer. These changes were overall consistent with the current climate patterns and scaled with the current climate amplitudes, with largest changes generally found in regions and for variables showing the largest amplitude in the current climate. Several regions displayed decreases in time mean or time variability: the northern Atlantic Ocean both in winter and summer, and the south of the domain and western Atlantic Ocean in summer. Changes were also comparable in relative terms for time mean and time variability, suggesting similar evolutions for both statistics. It also appeared that even small changes had to be considered, since they could correspond to large relative changes over cold and dry northern regions, where the largest relative changes were noted.

The contribution of the large and small scales to variability changes, as well as that of the CGCM-resolved and CGCM-unresolved terms for moisture flux divergence, also scaled overall with their contribution to current climate, with largest changes generally found for scales contributing more to time variability. Conversely, largest relative changes were often associated with scales contributing less to current climate. In summer results suggested that large scales would be more favoured to the north than to the south, which might be linked to shifting synoptic systems, while small scales would be more favoured to the southeast, maybe associated with more convection there.

Variability changes for the interaction terms entering the atmospheric water flux divergence were also consistent with current climate patterns; all terms showed an overall increased variability in the future climate, but without disturbing the balance between them. However, in terms of relative changes, some interaction terms appeared to be favoured. In winter, all terms presented relative increases exceeding 20% locally; but interactions involving the very large scales of wind or the small scales of humidity were favoured. In summer, all interaction terms showed relative variability changes more similar between each other, and smaller than in winter. But interactions involving the very large scales of wind seemed to be favoured to the north and interaction involving the small scales of humidity to the southeast.

Thus, in both the current atmospheric water budget climatology or its projected evolution, small scales appeared to contribute significantly to time variability, which suggests a strong added value from them. These transient small scales are associated with synoptic systems in winter and also convection in summer. Properly resolving them hence appears necessary for a proper representation and projection of changes in the hydrological extremes related to anthropogenic forcing. However these small scales should be compared to observed ones when possible to check their relevance to the observed climate. For now we can only infer a potential added value from the acknowledgement of their importance relative to large scales. However the great similarity of large- and small-scale patterns inspire confidence in the simulated small-scale fields.

The methodology used in this study is quite recent. Its positive results encourage to generalize it to other variables and budgets, such as the enstrophy or energy budgets, to gain more insight into the contribution of small scales to the maintenance of climate. While the small-scale contribution was important for the water budget variables, it might not be the case for other variables such as sea-level pressure or geopotential height (e.g., Feser 2006).

Acknowledgments This research was done as part of the Masters project of the first author and as a project within the Canadian Regional Climate Modelling and Diagnostics (CRCMD) Network, funded by the Canadian Foundation for Climate and Atmospheric Sciences (CFCAS) and the Ouranos Consortium for Regional Climatology and Adaptation to Climate Change. Ouranos also provided office space. We would like to thank Mr. Mourad Labassi for maintaining a user-friendly local computing facility. Thanks are also extended to the Ouranos Climate Simulation Team for their support of the CRCM software and for providing access to the climate simulations analysed here. Discussions with Dr. Soline Bielli have also been deeply appreciated. Finally, we would like to thank the three anonymous reviewers, whose suggestions contributed to improve the manuscript.

References

Allen MR, Ingram WJ (2002) Constraints on the future changes in climate and the hydrological cycle. Nature 419:224–232

Arakawa A, Lamb V (1977) Computational design of the basic dynamical processes of UCLA General Circulation Model. Methods in computational physics, vol 17. Academic Press, New York, pp 173–265

Bechtold P, Bazile E, Guichard F, Mascart P, Richard E (2001) A mass-flux convection scheme for regional and global models. Q J R Meteorol Soc 127:869–886

Bergeron G, Laprise L, Caya D (1994) Formulation of the Mesoscale Compressible Community (MC2) Model. Internal report from Cooperative Centre for Research in Mesometeorology, pp 165

Bielli S, Laprise R (2006) A methodology for the regional-scale-decomposed atmospheric water budget: application to a simulation of the Canadian Regional Climate Model nested by NCEP-NCAR reanalyses over North America. Mon Weather Rev 134:854–873

Bielli S, Laprise R (2007) Time mean and variability of the scale-decomposed atmospheric water budget in a 25-year simulation of the Canadian Regional Climate Model over North America. Clim Dyn 29:763–777

Boer GJ (1982) Diagnostic equations in isobaric coordinates. Mon Weather Rev 110:1801–1820

Boer GJ (1994) Mean and transient spectral energy and enstrophy budgets. J Atmos Sci 51:1765–1779

Boer GJ, Shepherd TG (1983) Large-scale two-dimensional turbulence in the atmosphere. J Atmos Sci 40:164–184

Boyd JP (2005) Limited-area Fourier spectral models and data analysis schemes: windows, Fourier extension, Davies relaxation, and all that. Mon Weather Rev 133:2030–2042

Caya D, Laprise R (1999) A semi-implicit semi-Lagrangian regional climate model: The Canadian RCM. Mon Weather Rev 127:341–362

Christensen JH, Hewitson B, Busuioc A, Chen A, Gao X, Held I, Jones R, Kolli RK, Kwon W-T, Laprise R, Magaña Rueda V, Mearns L, Menéndez CG, Räisänen J, Rinke A, Sarr A, Whetton P (2007) Regional climate projections. In: Solomon S, Qin D, Manning M, Chen Z, Marquis M, Averyt KB, Tignor M, Miller HL (eds) Climate change 2007: the physical science basis. Contribution of Working Group I to the fourth assessment report of the Intergovernmental Panel on Climate Change. Cambridge University Press, Cambridge

Davies HC (1976) A lateral boundary formulation for multi-level prediction models. Q J R Meteorol Soc 102:405–418
Denis B, Côté J, Laprise R (2002) Spectral decomposition of two-dimensional atmospheric fields on limited-area domains using the discrete cosine transform (DCT). Mon Weather Rev 130:1812–1829
Efron B, Tibshirani TJ (1993) An introduction to the bootstrap. Chapman and Hall, Norwell, p 436
Errico RM (1985) Spectra computed from a limited area grid. Mon Weather Rev 113:1554–1562
Feser F (2006) Enhanced detectability of added value in limited-area model results separated into different spatial scales. Mon Weather Rev 134:2180–2190
Flato GM, Boer GJ (2001) Warming asymmetry in climate change simulations. Geophys Res Lett 28:195–198
Gal-Chen T, Somerville RCJ (1975) On the use of a coordinate transformation for the solution of the Navier–Stokes equations. J Comp Phys 17:209–228
Giorgi F, Marinucci MR (1996) An investigation of the sensitivity of simulated precipitation to model resolution and its implications for climate studies. Mon Weather Rev 124:148–166
Iorio JP, Duffy PB, Govindasamy B, Thompson SL, Khairoutdinov M, Randall D (2004) Effects of model resolution and subgrid-scale physics on the simulation of precipitation in the continental United States. Clim Dyn 23:243–258
Kain JS, Fritsch JM (1990) A one-dimensional entraining/detraining plume model and application in convective parameterization. J Atmos Sci 47:2784–2802
Laprise R (1992) The resolution of global spectral models. Bull Am Meteorol Soc 73:1453–1454
Laprise R (2003) Resolved scales and nonlinear interactions in limited-area models. J Atmos Sci 60:768–779
Laprise R (2008) Regional climate modelling. J Comp Phys 227:3641–3666 Special issue on « Predicting weather, climate and extreme events »
Laprise R, Girard C (1990) A spectral general circulation model using a piecewise-constant finite element representation on a hybrid vertical coordinate system. J Clim 3:32–52
Laprise R, Caya D, Bergeron G, Giguère M (1997) The formulation of André Robert MC2 (mesoscale compressible community) model. Atmos Ocean 35:195–220
Lawford RG, Stewart R, Roads J, Isemer H-J, Manton M, Marengo J, Yasunari T, Benedict S, Koike T, Williams S (2004) Advancing global- and continental-scale hydrometeorology: contributions of GEWEX hydrometeorology panel. Bull Am Meteorol Soc 85:1917–1930
Lawford RG, Roads J, Lettenmaier DP, Arkin P (2007) GEWEX contributions to large-scale hydrometeorology. J Hydrometeor 8:629–641
McFarlane NA, Scinocca JF, Lazare M, Harvey R, Verseghy D, Li J (2005) The CCCma third generation atmospheric general circulation model. CCCma internal report, pp 25
Music B, Caya D (2007) Evaluation of the hydrological cycle over the Mississippi River basin as simulated by the Canadian Regional Climate Model (CRCM). J Hydrometeor 8:969–988
Music B, Caya D (2009) Investigation of the sensitivity of water cycle components simulated by the Canadian Regional Climate Model (CRCM) to the land surface parameterization, the lateral boundary data and the internal variability. J Hydrometeor 10:3–21
Nakicenovich N et al (2000) IPCC special report on emissions scenarios. Cambridge University Press, Cambridge, p 599
Paquin D, Caya D (2000) New convection scheme in the Canadian Regional Climate Model. Res Act Atmos Ocean Model 30:7.14–7.15
Peixoto J, Oort A (1992) Physics of climate. American Institute of Physics, USA, p 520
Riette S, Caya D (2002) Sensitivity of short simulations to the various parameters in the new CRCM spectral nudging. Res Act Atmos Ocean Model 32:7.39–7.40
Scinocca JF, McFarlane NA (2004) The variability of modelled tropical precipitation. J Atmos Sci 61:1993–2015
Trenberth KE (1998) Atmospheric moisture residence times and cycling: implications for rainfall rates with climate change. Clim Change 39:667–694
Trenberth KE (1999a) Conceptual framework for changes of extremes of the hydrological cycle with climate change. Clim Change 42:327–339
Trenberth KE (1999b) Atmospheric moisture recycling: role of advection and local evaporation. J Clim 12:1368–1381
Trenberth KE, Dai A, Rasmussen RM, Parsons DB (2003) The changing character of precipitation. Bull Am Meteorol Soc 84:1205–1217
Van Tuyl AH, Errico RM (1989) Scale interaction and predictability in a mesoscale model. Mon Weather Rev 117:495–517
Verseghy DL (1991) CLASS—a Canadian Land Surface Scheme for GCMs. Part I: soil model. Int J Climatol 11:111–113
Verseghy DL, McFarlane NA, Lazare M (1993) CLASS—a Canadian Land Surface Scheme for GCMs. Part II: vegetation model and coupled runs. Int J Climatol 13:347–370
Yakimiw E, Robert A (1990) Validation experiments for a nested grid-point regional forecast model. Atmos Ocean 28:466–472